Geophysical Journal International

Geophys. J. Int. (2013) **192,** 871–887 doi: 10.1093/gji/ggs065

Australian Seismological Reference Model (AuSREM): mantle component

B. L. N. Kennett,[1] A. Fichtner,[2] S. Fishwick[3] and K. Yoshizawa[4]

[1]*Research School of Earth Sciences, The Australian National University, Canberra ACT* 0200*, Australia. E-mail: Brian.Kennett@anu.edu.au*
[2]*Department of Earth Sciences, Utrecht University, Budapestlaan* 4, 3584 CD*, Utrecht, The Netherlands*
[3]*Department of Geology, University of Leicester, University Road, Leicester,* LE1 7RH*, UK*
[4]*Earth and Planetary Dynamics, Department of Natural History Sciences, Graduate School of Science, Hokkaido University,* N10W8 *Kita-ku, Sapporo* 060810*, Japan*

Accepted 2012 November 6. Received 2012 October 22; in original form 2012 July 9

SUMMARY

The mantle component of the Australian Seismological Reference Model (AuSREM) has been constructed from Australian-specific sources, primarily exploiting the wealth of seismic sources at regional distances around Australia recorded at portable and permanent stations on the continent. AuSREM is designed to bring together the existing information on Australia, from both body wave and surface wave studies and provide a synthesis in the form of a 3-D model that can provide the basis for future refinement. The model is grid based with a 0.5° sampling in latitude and longitude, and is designed to be fully interpolable, so that properties can be extracted at any point.

For the upper mantle the primary source of information comes from seismic surface wave tomography, supplemented by analysis of body wave arrivals and regional tomography which provide useful constraints on the relation between *P*- and *S*-wave speeds in the mantle lithosphere. A representative model has been developed to capture the features of mantle structure drawing on a range of studies. The mantle structure is represented by grid values at 25 km intervals in depth from 75 to 300 km. Shallower structure is linked to the AuSREM crust through the recent Moho depth model of Kennett *et al.*, which exploits all available sources of seismological information. Below 300 km depth and in the surrounding area AuSREM is linked to the *S40RTS* model of Ritsema *et al.*

Key words: Mantle processes; Body waves; Surface waves and free oscillations; Seismic tomography; Australia.

GJI Seismology

1 INTRODUCTION

There have been a wide range of studies of the upper mantle beneath Australia exploiting the large amplitude surface waves and multiple *S* waves in the later parts of seismograms from events in the earthquake belts around Australia. These studies have exploited recordings at portable broad-band seismic stations and the limited number of high-quality permanent stations (see, e.g. Debayle & Kennett 2003). Now full continental coverage is available, the large-scale features of wave speed structure are well delineated, and agree well with results from body wave studies at much higher frequency.

The mantle component of the Australian Seismological Reference Model (AuSREM) is built from a suite of estimates of mantle structure based on different styles of analysis and inversion, and incorporates constraints from both surface and body wave studies, as well as delay time tomography. The aim is to provide a representation of the 3-D structure in the mantle beneath Australia and its environs that captures the major features of the structure in a form that can be used in a range of applications, and provide a starting point for more detailed work.

A general description of the AuSREM project is given by Kennett & Salmon (2012), and a detailed discussion of the construction of the crustal component is to be found in Salmon *et al.* (2012). The first phase of the work was the generation of a new model for Moho depth exploiting the full range of relevant seismological information (Kennett *et al.* 2011), and this Moho distribution provides the link between the crustal and mantle components of AuSREM. The reference model is built on the full range of crustal and mantle studies using Australian-specific information, the aim is to provide a model which captures the major features of lithospheric structure as revealed by both seismic body wave and surface wave studies, and hence is suitable for geodynamic interpretation. Potential applications of AuSREM include the delineation of major structural features and improved earthquake source characterization, both within Australia and at the immediate plate boundaries by using better representations of crustal and mantle structure in source inversion and event location.

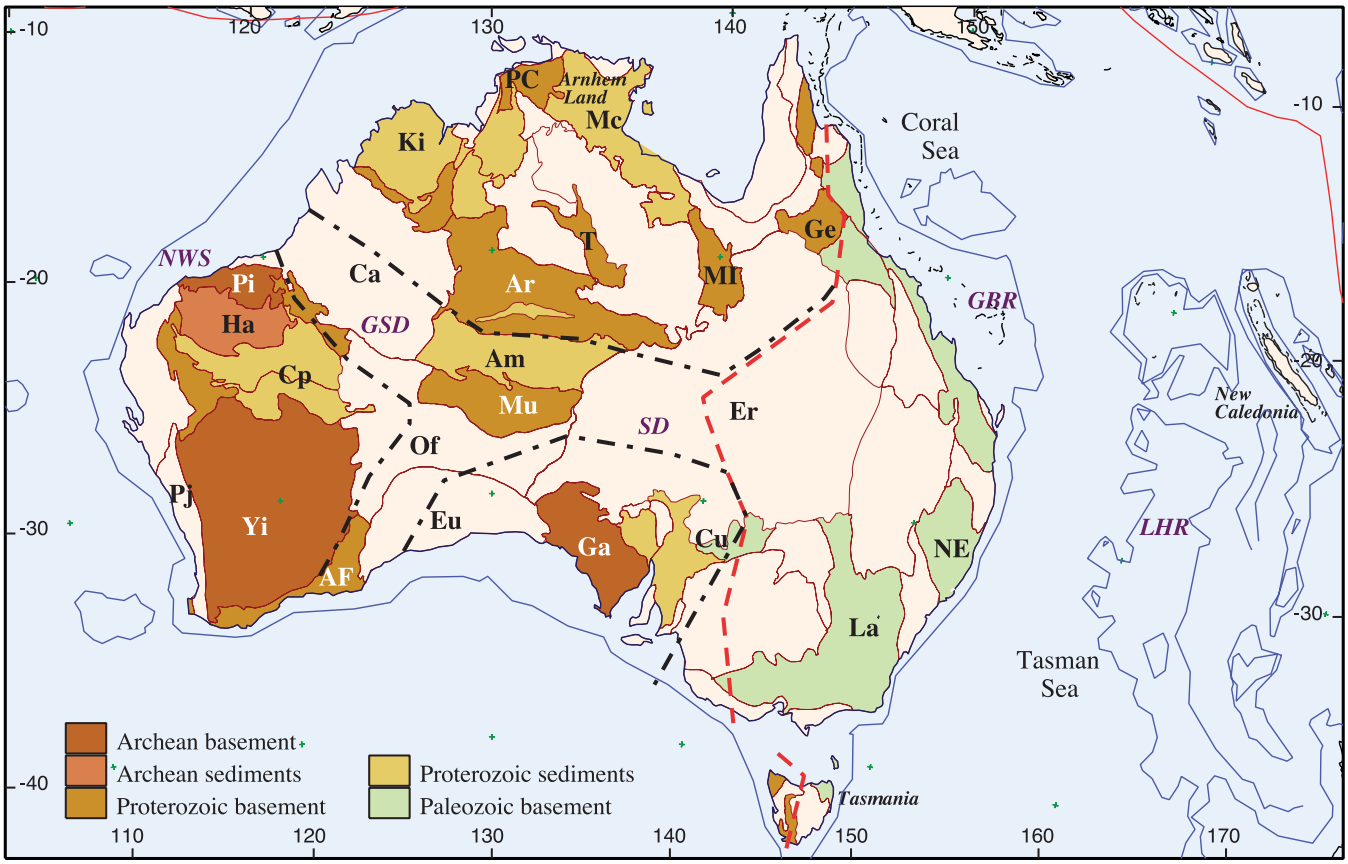

Figure 1. Simplified representation of the main tectonic features of Australia and its surroundings. The outline of the major cratons are marked by chain-dotted lines. The Tasman line in red is based on the reinterpretation by Direen & Crawford (2003). Key to marked features: AF, Albany-Fraser belt; Ar, Arunta Block; Am, Amadeus Basin; Ca, Canning Basin; Cp, Capricorn Orogen; Cu, Curnamona Craton; Er, Eromanga Basin; Eu, Eucla Basin; Ga, Gawler Craton; Ge, Georgetown inlier; Ha, Hamersley Basin; Ki, Kimberley Block; La, Lachlan Orogen; Mc, MacArthur Basin; MI, Mt Isa Block; Mu, Musgrave Block; NE, New England Orogen; Of, Officer Basin; PC, Pine Creek Inlier; Pi, Pilbara Craton; Pj, Pinjarra Orogen; T, Tennant Creek Block; Yi, Yilgarn Craton; *NWS*, Northwest Shelf; *GBR*, Great Barrier Reef; *LHR*, Lord Howe Rise; *SD*, Simpson Desert; *GSD*, Great Sandy Desert.

1.1 Tectonic setting

The exposed geology of the Australian continent is composed of an assemblage of crustal blocks that can be broadly grouped into the Precambrian western and central cratonic zones and the Phanerozoic eastern province (Fig. 1). Cratonic fusion was complete by around 1900 Ma, and the Precambrian core was left after the break up of Rodinia around 800 Ma. The east of Australia was an accretionary margin through the Palaeozoic with a sequence of subduction complexes on the margin of Gondwana progressively building to the east. Australia parted company with East Antarctica by around 80 Ma, and later the opening of the Tasman Sea from 80 to 60 Ma separated the Lord Howe Rise from eastern Australia to leave a submerged continental ribbon. Neogene volcanism along the eastern margin has left chains of volcanic edifices on land and in the Tasman sea, with eruptions as recent as 4000 BCE at Mt Gambier (38°S, 141°E).

The tectonic assemblage has left its imprint on the mantle. Thick lithosphere with high seismic wave speed lies beneath the centre and west of the continent, and much thinner lithosphere is present in the east and into the Tasman Sea (see e.g. Fishwick *et al.* 2008).

2 DATA SOURCES

Major earthquake belts are associated with the subduction zones to the north and east of Australia from Indonesia to Vanuatu and the Tonga-Kermadec system, through New Zealand and into the Macquarie ridge. Less frequent seismicity occurs on the mid-ocean ridge between Australia and Antarctica. These earthquakes along the Australian Plate margins provide events that lie at suitable distances from stations on the continent to be used as probes for upper- mantle structure. The frequency of regional events is high, and so good coverage can be achieved in a few months. This has enabled campaigns of deployments of portable broad-band stations to supplement the limited number of high-fidelity permanent stations. The systematic use of portable stations was pioneered with the SKIPPY experiment (van der Hilst *et al.* 1994), where a group of stations were progressively moved across the continent in a sequence of deployments. Since 2005 number of new permanent stations have been installed by Geoscience Australia as part of an enhanced tsunami warming system, and these provide a useful supplement to the available data.

The combination of a long duration of recording at the permanent stations, and the broad spatial coverage from the portable stations provides an excellent resource for studies of the lithosphere. A wide range of techniques exploiting different aspects of seismograms, have been employed to extract information on the 3-D structure in the crust and mantle. These studies have used both the large amplitude surface wave components, but also higher frequency body waves in a variety of ways.

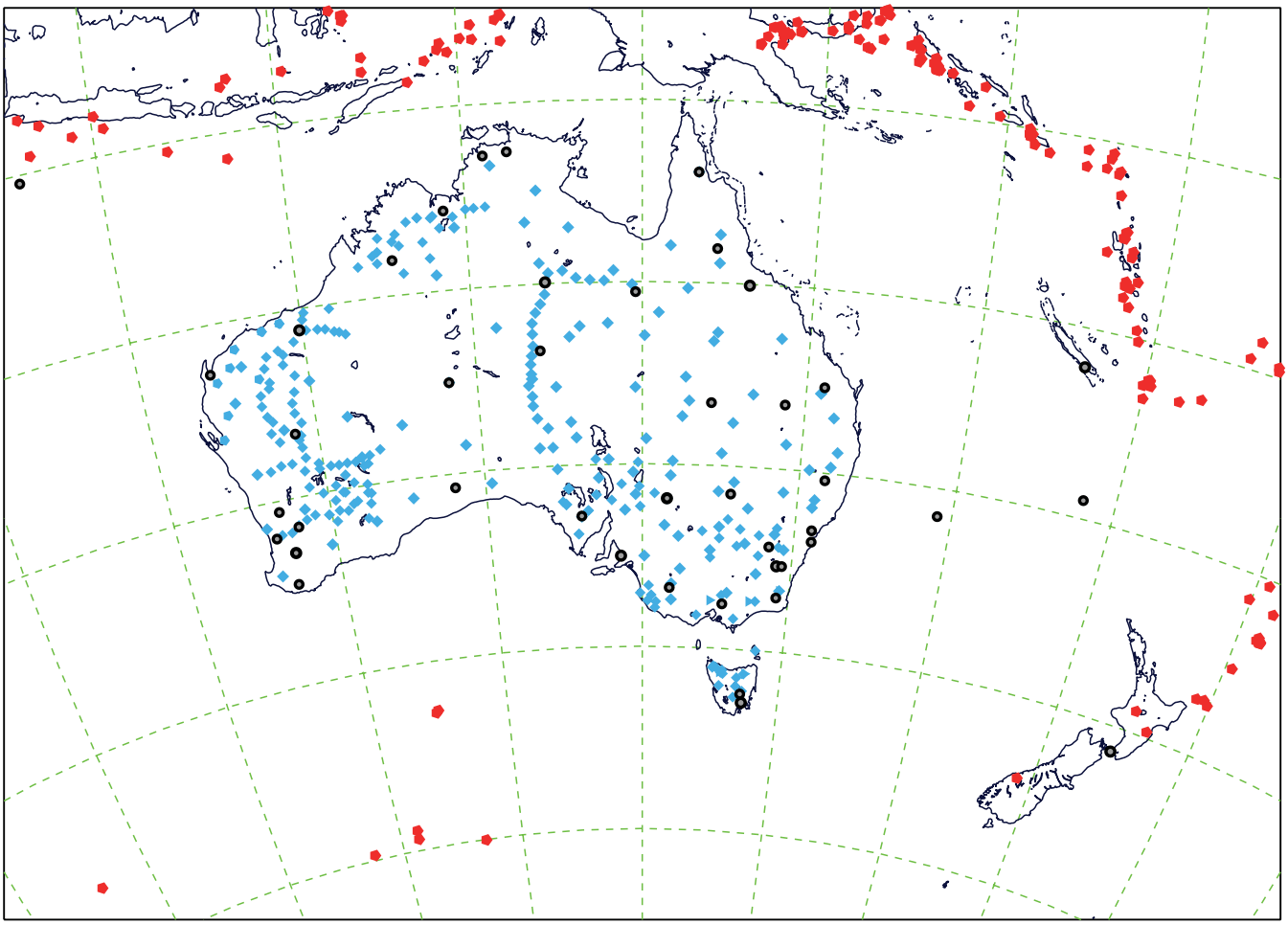

Figure 2. Configuration of seismic stations in Australia, permanent stations are shown in black and the portable broad-band stations in blue, together with seismic events with $M_s \geq 5$ for the year 2001, to illustrate the potential coverage.

In addition to the broad-band studies, much denser deployments of shorter period stations have been made in southeastern Australia since 1999. These stations have mainly been employed in tomographic studies of the crust and uppermost mantle. Initially studies were made from the individual deployments, but the data from the whole sequence of station arrays has now been brought together in the WOMBAT project (Rawlinson *et al.* 2011).

The combination of the permanent and portable stations in Australia and its neighbours (Fig. 2), with the wealth of regional earthquakes provides a configuration in which good sampling of the continent can be achieved. The absence of a regular supply of earthquakes to the west means that there is limited east–west control on the western margin of Australia. In contrast the area of the northern Tasman Sea on the eastern margin has excellent multidirectional coverage.

2.1 Prior studies

Much of what we know about the upper-mantle structure under Australia has come from the exploitation of the multiple reflected shear waves and surface waves from regional earthquakes. These phases form the most prominent part of seismograms in the period range from 20 to 200 s. A variety of techniques have been employed to extract information on 3-D structure. One approach is to extract path-specific velocity models using either direct inversion of a portion of the seismogram (e.g. Simons *et al.* 2002), or secondary variables that improve the linearity of the inversion (e.g. Debayle & Kennett 2003; Fishwick *et al.* 2005) . These path-based models can then be combined in a linear inversion for 3-D shear wave speed structure. An alternative approach via the construction of phase speed maps for multiple modes and frequencies allows the incorporation of finite-frequency sampling (Yoshizawa & Kennett 2004). The most sophisticated approach is a fully non-linear inversion of the waveforms using 3-D models from the outset (Fichtner *et al.* 2009, 2010). This computationally intensive approach has been based on the spectral element technique for modelling the wave propagation and adjoint methods to extract the necessary derivatives, which naturally include all finite-frequency effects.

The result of this range of different approaches is that structural variations have been imaged on scales down to 250 km horizontally and 30 km vertically. Significant substructure appears within the zones of both higher and lowered wave speeds (Figs 3 and 4). The major features of all the recent models are concordant, and this provides the basis for constructing a representative model.

We also have information from studies of body waves at much higher frequencies from the same regional sources. Kaiho & Kennett (2000) undertook a study of refracted waves through the upper mantle. They built record sections for a suite of corridors across the continent, and then used this information to extract 3-D structure under northern Australia for both *P*- and *S*-wave speeds.

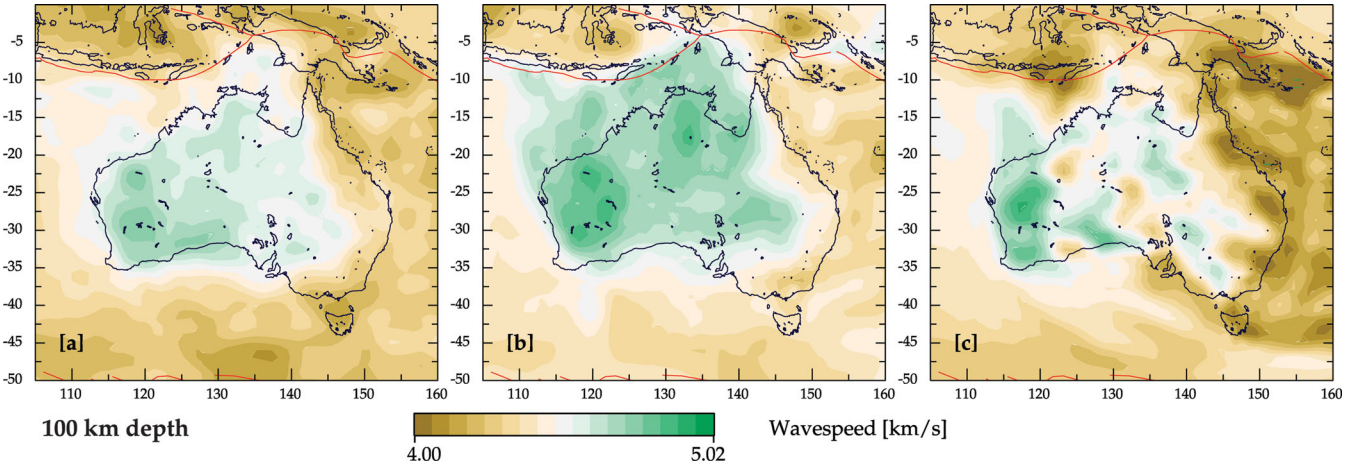

Figure 3. Shear wave speed for the three base *SV* models at 100 km depth: (a) from Fishwick *et al.* (2008), (b) an update of the Yoshizawa & Kennett (2004) model and (c) from Fichtner *et al.* (2010) from full 3-D waveform inversion.

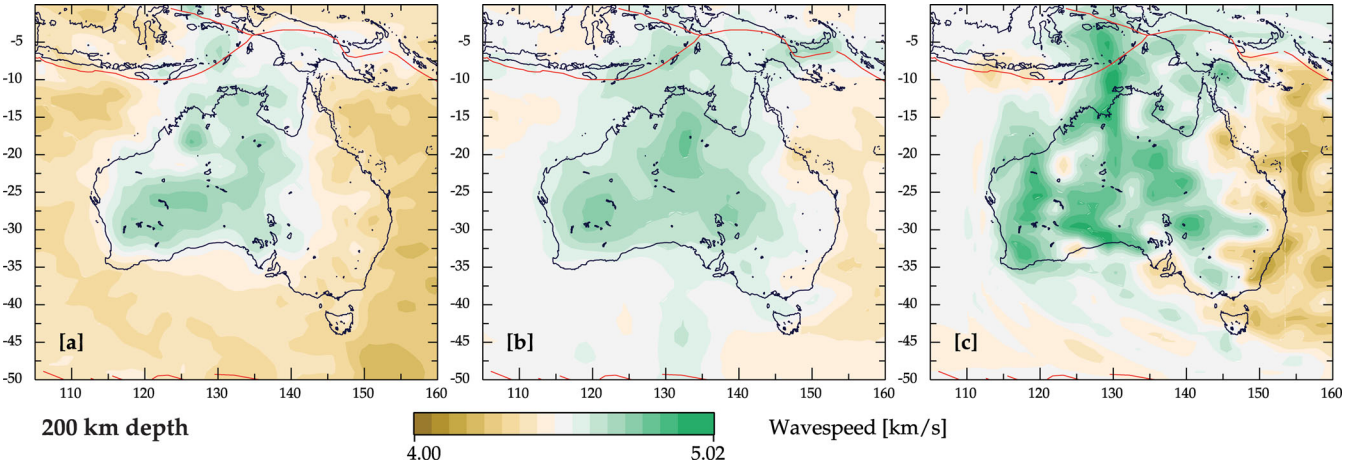

Figure 4. Shear wave speed for the three base *SV* models at 200 km depth: (a) from Fishwick *et al.* (2008), (b) an update of the Yoshizawa & Kennett (2004) model and (c) from Fichtner *et al.* (2010) from full 3-D waveform inversion.

This work provides valuable information on the relation between *P*- and *S*-wave speeds and its likely geographical variation. Subsequently tomographic inversion for the refracted phases has been conducted for both *P*- and *S*-wave speeds, in the context of studying the attenuation structure beneath the Australian region (Kennett & Abdulah 2011).

In addition we can make use of tomographic inversions carried out using principally teleseismic arrivals for both *P* and *S* waves (e.g. Gorbatov & Kennett 2003). Such studies provide good horizontal resolution, but the limited range of angles of incidence means that there is a tendency for some smearing of structure in the vertical direction.

3 LITHOSPHERIC MODEL

There are two different approaches that can be employed to develop a reference model. The first is to use a specific inversion based on one style of information using as comprehensive a coverage as possible. For instance, Schivardi & Morelli (2011) inverted for mantle structure using group velocity information for the European region exploiting the improved crustal model developed by Molinari & Morelli (2011). In this way a model is secured that is firmly linked to a particular data set, but which may well not be as effective when used for other purposes. The second approach is to build on a compilation of structural information from a variety of sources to extract a model that includes elements from many different sources. This second style of model has been commonly used in crustal studies (e.g. Molinari & Morelli 2011; Salmon *et al.* 2013), and has the merit of building on all available sources of information. However, the resulting model may well not fit any specific data set as well as a model constructed for the purpose.

Rather than undertake a new inversion, we build on the information available from previous studies to build a representative model for the mantle component of AuSREM. The general consistency between the different models from surface wave studies and the results from body waves means that the major features of the structure are well defined, and this forms the basis of our construction of the AuSREM mantle model. There are differences in smaller scale features and we anticipate that subsequent work will require revision in detail, but the present model should be a suitable starting point for, for example, inversion for 3-D structure. Our primary source of information is for shear wave speed, but we construct *P*-wave speed, density and attenuation models using information from body wave studies and petrological models.

The AuSREM mantle model is specified in terms of absolute velocities and densities since this is what is needed for many applications. The primary model nodes are at 0.5° spacing in latitude

and longitude and 25 km spacing in depth from 75 to 300 km. A 50-km slice cuts the Moho in a few places across the continent (Kennett *et al.* 2011). Crustal influences on estimates of mantle structure are rather strong at this depth, but should be moderated by the way we have combined models with various approaches to the representation of crustal structure and consequently different crustal influences. To provide control at 50 km depth, we have combined the mantle *SV* model with a smoothed version of the *S*-wave model from the crust (Salmon *et al.* 2012).

We start from three shear wave speed models for the mantle in the Australian region based on very different approaches to the analysis of seismograms from regional earthquakes. We illustrate these models at depths of 100 km and 200 km in Figs 3 and 4. We have used these shear wave speed models as the primary information because they provide full continental coverage. The path coverage associated with each of the models is displayed in the Supporting Information (Fig. S1). The disposition of available earthquakes means that path coverage drops off to the west of the Australian continent. The three models illustrated in Figs 3 and 4 use different approaches to the exploitation of seismic waveforms as well as different data sets. Nonetheless the broad outlines of the wave speed structure are similar, and are in close concordance for the longer spatial wavelengths (Fichtner *et al.* 2012).

The first model is taken from Fishwick & Rawlinson (2012), building on the previous work of Fishwick *et al.* (2008), but with the inclusion of significantly more data. Path-specific 1-D models are constructed using inversion for the fundamental Rayleigh mode and first few higher modes via the secondary variable approach of Cara & Lévêque (1987). The 1-D models are then combined in a linear inversion with regularization to produce a series of depth slices at 25 km intervals. In this approach there is a strong influence from the fundamental Rayleigh mode and so sensitivity tends to diminish at depths below 250 km. The latest model exploits data from permanent and portable stations across both the Australian continent and the surrounding regions, resulting in over 13 000 paths included within the tomographic inversion. Excellent path coverage and azimuthal distribution is observed in the centre and east of Australia, while the inclusion of Geoscience Australia stations has significantly improved coverage in the west (Fishwick & Rawlinson 2012).

The second model is based on a three-stage approach (Yoshizawa & Kennett 2004) with the inclusion of additional paths and allowance for radial anisotropy. A fully non-linear waveform inversion is undertaken using the Neighbourhood Algorithm (Sambridge 1999). The criterion for matching the long-period multiple *S* waves and surface waves is based on a combination of envelope and phase fit in multiple time–frequency windows (Yoshizawa & Kennett 2002; Yoshizawa & Ekström 2010). Path-specific models from the non-linear inversion are then interpreted as summaries of multimode dispersion. The reliability of estimated dispersion is evaluated by the relative modal strength and waveform fit in a time–frequency domain. A cluster analysis is then employed for eliminating outlying measurements (Yoshizawa & Ekström 2010), and eventually over 8000 paths for the fundamental mode and about 2000 paths for the higher modes are collected. For each mode a set of phase-speed maps are constructed as a function of frequency, incorporating possible off-great circle propagation and the influence zone around the propagation path which varies with frequency. Local dispersion curves are extracted and an inversion is made for a local 1-D model. Finally a 3-D model is assembled from the ensemble of local models.

The third model is taken from the work of Fichtner *et al.* (2010) where inversion for a radially anisotropic model is made using a linearized inversion with 3-D waveform modelling at each step, constructed using the spectral element method and an adjoint construction for the necessary derivatives for the frequency–time domain waveform fit criterion. A smooth 3-D starting model was based on the work of Fishwick *et al.* (2005) for wave speeds and used the attenuation model presented in Kennett & Abdulah (2011). This is the most sophisticated and computationally intensive of the three methods and requires good calibration of the instrumental responses for the seismograms employed. More paths are brought in as the inversion proceeds so that the corresponding traces are sufficiently well represented that they can contribute to 3-D model improvement at the next iteration. Nevertheless the number of controlling paths (about 800) is less than in the other models, and azimuth control is limited on the western edge of the continent. Through fits to the multiple *S* phases (higher modes) the spectral element approach can provide information to considerable depth. Anomalies at 200 km and below tend to be somewhat larger than for the other methods, but the more limited sampling can induce quite strong local gradients, even though finite-frequency effects are naturally included in the full 3-D inversion.

In addition to the differences in inversion methodology, the three models illustrated in Figs 3 and 4 use different approaches to accounting for the crust, from path averages to a specially designed composite element for the spectral element method (Fichtner & Igel 2008). Nonetheless the broad outlines of the structure are similar, and the resemblances increase when appropriate spatial filtering is applied to extract the longer spatial wavelengths (Fichtner *et al.* 2012). In constructing the AuSREM mantle model we seek to produce a representation where the major features are robust. We have therefore employed linear combinations of the shear wave speed models to emphasize such features. Smaller scale features will tend to be suppressed even though they may be required, or introduced, by a particular data set and inversion scheme.

We have independent confirmation of the spatial configurations of fast and slower seismic wave speeds from delay time tomography, which exploits teleseismic arrivals as well as those from regional events. In the absence of significant local events the majority of propagation paths travel rather steeply through the upper part of the mantle, and the attainable resolution is dictated by station coverage. In Fig. 5 we show the results of *P* and *S* tomography using the approach described by Gorbatov & Kennett (2003). The results are displayed as deviations from the *ak135* model of Kennett *et al.* (1995). To allow for the stretching in the tomographic model induced by the narrow cone of sampling of the incident waves at the stations we present the images at 110 and 220 km for comparison with surface wave models at 100 and 200 km. This 10 per cent correction gives a slight improvement in the correspondence between the two sets of results in the areas where we have adequate sampling. Localized station information, as in the the recent WOMBAT arrays in southeastern Australia for *P* waves, can bring in details that cannot be captured by the longer wavelengths employed in surface wave tomography (e.g. Fishwick & Rawlinson 2012).

Additional valuable information on *P*-wave speed behaviour comes from the study of refracted body waves undertaken by Kaiho & Kennett (2000). They concentrated on a suite of corridors across the continent using events to the north and east of Australia, and were able to build corridor-specific velocity models from analysis of the waveform, especially the nature of triplications arising from the upper-mantle discontinuities. The wave speeds from the various corridors were then brought together in a 3-D synthesis as

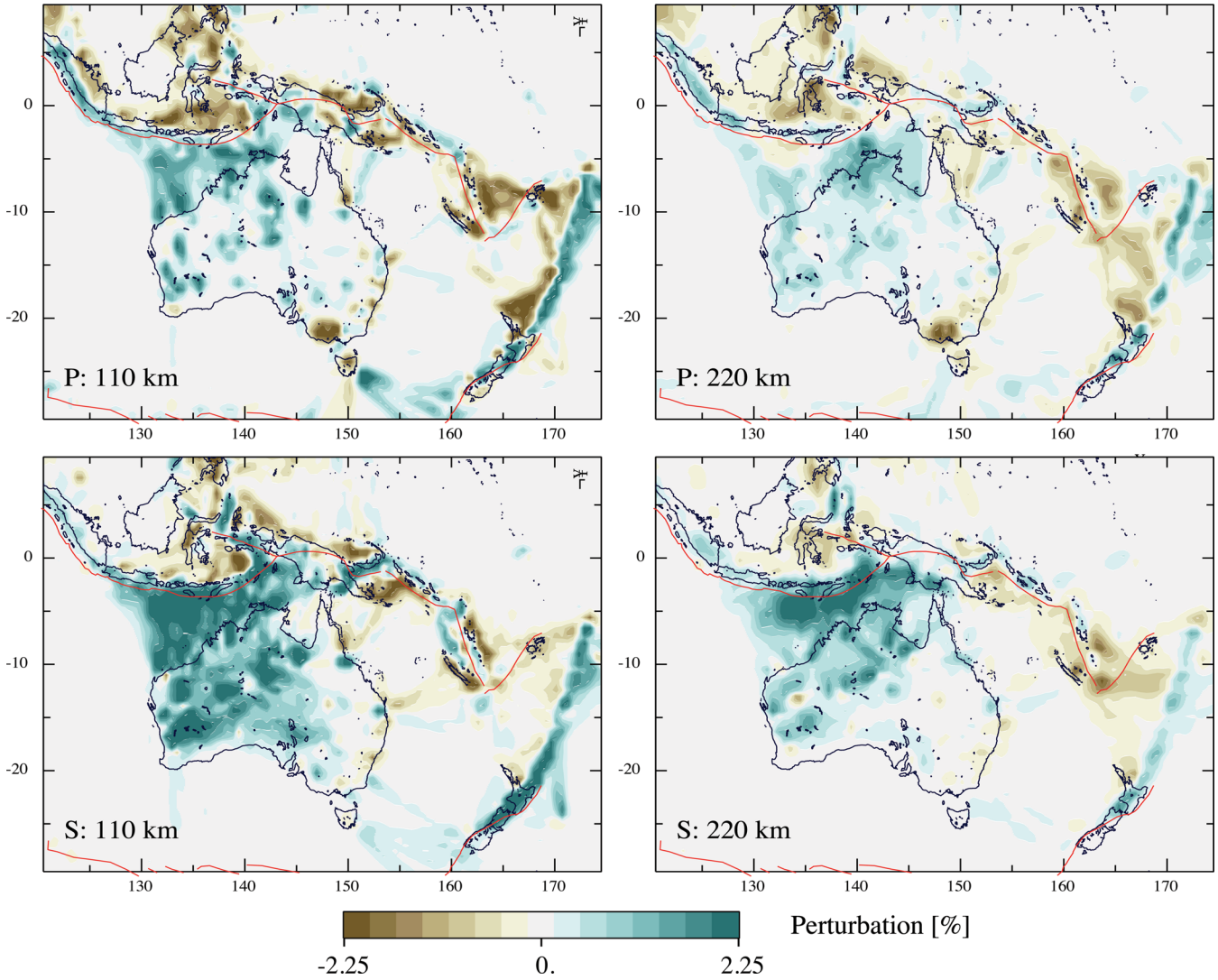

Figure 5. *P*- and *S*-wave tomography from body waves arrivals using the approach of Gorbatov & Kennett (2003). Slices are shown at 110 and 220 km to compare with Figs 3 and 4, allowing for the vertical stretching in the tomographic image. The images are displayed as perturbations from the *ak135* model of Kennett *et al.* (1995).

illustrated in Fig. 6. In addition we have assembled a set of traveltime information for well-characterized paths traversing the Australian lithosphere for both *P* and *S* waves, building on the results of Kaiho & Kennett (2000) with later supplements (see Figs S2 and S3). In particular, coverage of *P* waves is enhanced by studies of particularly well-located earthquakes undertaken by Geoscience Australia (S. Spiliopolous, personal communication, 2005).

P-wave speed variations from *ak135* are significantly smaller than for *S*. We use the information from the studies presented in Figs 5, 6, S2 and S3 together with results from the tomographic study of Kennett & Abdulah (2011) to generate a suitable scaling relation between the wave speed distributions. We have used a single relation for simplicity, in the absence of full control on the geographic variations in the *P*-wave speed distribution.

3.1 Shear wave speed

We have constructed a representative radially anisotropic model for the shear wave speeds in the Australian mantle by using a weighted combination of the *SV* wave models and their *SH* wave counterparts, designed to also represent the body wave constraints. Our objective is to capture the main features of the lithosphere, and so by combining multiple models we reduce the dependence on the specific mode of inversion and the data coverage. As we have noted earlier, the longer spatial wavelength components of the three different studies are in good agreement as to the patterns of behaviour in the mantle, with fast *S*-wave speeds in the west and centre of the continent and lower wave speeds in the east and into the Tasman Sea. Differences in the size of the variations can be associated with the nature of the regularization employed, and the influence of finite frequency. The construction of the composite model tends to suppress small-scale heterogeneities that are not well resolved. We recognize that such a composite model need not provide as close a fit to a particular data set as provided by the model constructed directly from this data set Yet, by virtue of having multiple sets of path coverage and different analysis techniques, the composite model tends to minimize the influence of minor features that may be data set specific. Thus, the reference model should provide a good starting point for future inversions, because it emphasizes the robust features of the structure beneath the continent and its environs.

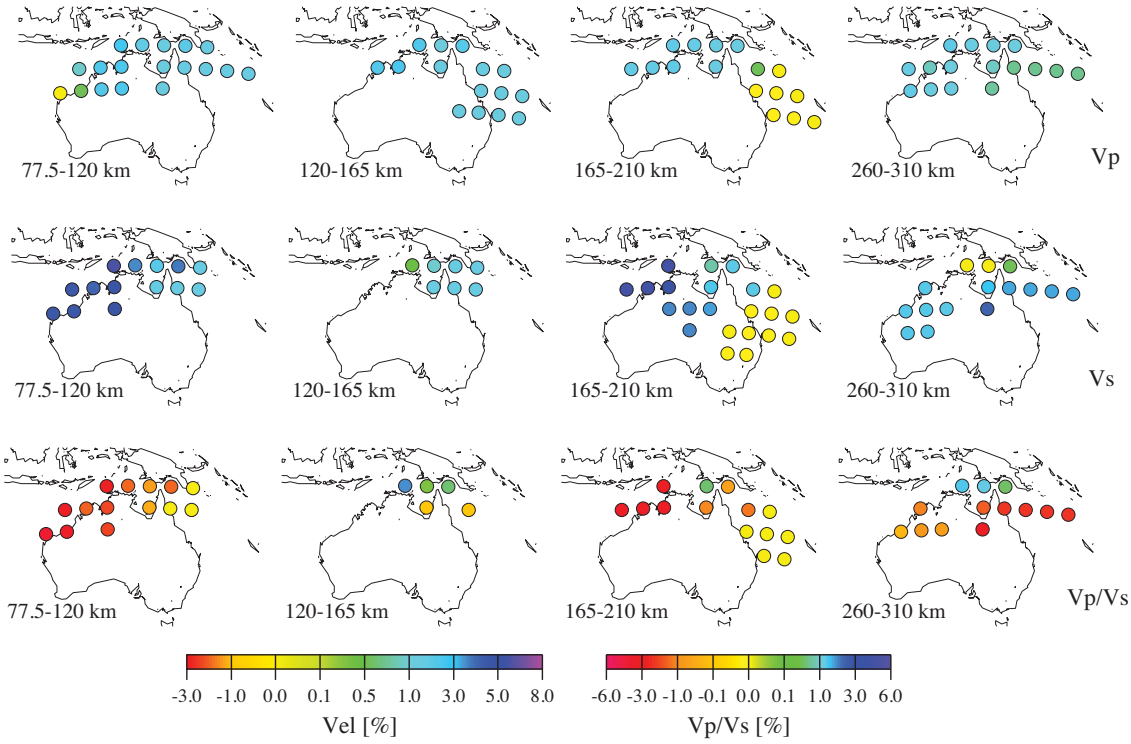

Figure 6. *P*- and *S*-wave speed perturbations from the *ak135* model, and deviations in the *P*- to *S*-wave speed ratio determined from studies of refracted body waves (Kaiho & Kennett 2000).

There is considerable evidence for azimuthal anisotropy in the propagation of fundamental mode Rayleigh waves across the Australian continent (e.g. Debayle *et al.* 2005; Fishwick *et al.* 2008) with a change in dominant fast wave speed direction from east–west at 100 km depth to nearly north–south at 200 km depth. Such studies suggest that less than 15 per cent of the total variation in *SV* wave speed could be attributable to azimuthal variation. We have decided against trying to include such azimuthal effects in the reference model. To do so in a fully consistent way would require a rather complex anisotropic model that would be very difficult to use for general purposes. We have, however, incorporated polarization anisotropy with separate *SV* and *SH* wave models, equivalent to transverse isotropy with a vertical symmetry axis.

The reference model is based on the suite of models displayed in Figs 3 and 4 taken in conjunction with the body wave results. The latest shear wave speed models from waveform inversion incorporate more of the Geoscience Australia permanent stations and portable stations deployed since the earlier studies (Yoshizawa & Kennett 2004; Fishwick *et al.* 2008). These updates significantly improve the path coverage, especially in the west, see Fig. S1. The models are used without spatial filtering, and we construct a weighted sum. We have given modest emphasis to the studies with the highest path density, while recognizing the benefits arising from improved representations of finite-frequency and 3-D effects. A number of candidate models were prepared and the selection of the reference was made based on preferred character across the range of depths, and compatibility with body wave constraints where they are available. Any process of selecting weights between different models will have some subjective component, but our aim has been to produce a representative model that is generally smooth and captures the main long wavelength features, yet presents detail where the diverse models and data sources concur.

The final weighting for the *SV* wave speed reference model $\beta^V_{\rm ref}$ at depths from 75 to 300 km is

$$\beta^V_{\rm ref}(z) = 0.38\beta^V_{\rm F}(z) + 0.37\beta^V_{\rm Y}(z) + 0.25\beta^V_{\rm W}(z), \quad (1)$$

where $\beta_{\rm F}$ is the updated Fishwick model, $\beta_{\rm Y}$ is the updated Yoshizawa model and $\beta_{\rm W}$ comes from the full-waveform inversion of Fichtner *et al.* (2010).

The *SV* model is well constrained and we can have considerable confidence in the main features (Fig. 7). The principal differences in the constituent models arise in variability in the shallower parts of the mantle near the western margin of Australia, where path sampling is both less and also less well distributed azimuthally (see Fig. S1). The AuSREM mantle representation is designed to cover the full range of seismic frequencies and so the choice of model combinations has been guided by consistency with body wave results (as in Figs 5, 6, S2 and S3). We recognize that there will be modifications needed in the future in the light of new information. Indeed a major role for a reference model is to assist in the development of such new studies.

We have less control on the *SH* wave distribution, and in this case we have to recognize that there are some discrepancies between the base models. Nevertheless, we feel that the *SH* model illustrated in Fig. 8 is suitably representative of the main features of the wave speed in 3-D. This *SH* reference model $\beta^H_{\rm ref}$ has been constructed with the weighting

$$\beta^H_{\rm ref}(z) = 0.6\beta^H_{\rm Y}(z) + 0.4\beta^H_{\rm W}(z), \quad (2)$$

which places greater emphasis on the model with broader path coverage particularly in the west, but allows detail to be introduced from the full waveform-inversion study.

The *SH* model displayed in Fig. 8 uses direct information from the prior models, but tends to have shorter wavelength features than the *SV* model. In consequence the distribution of the *SH*/*SV* wave

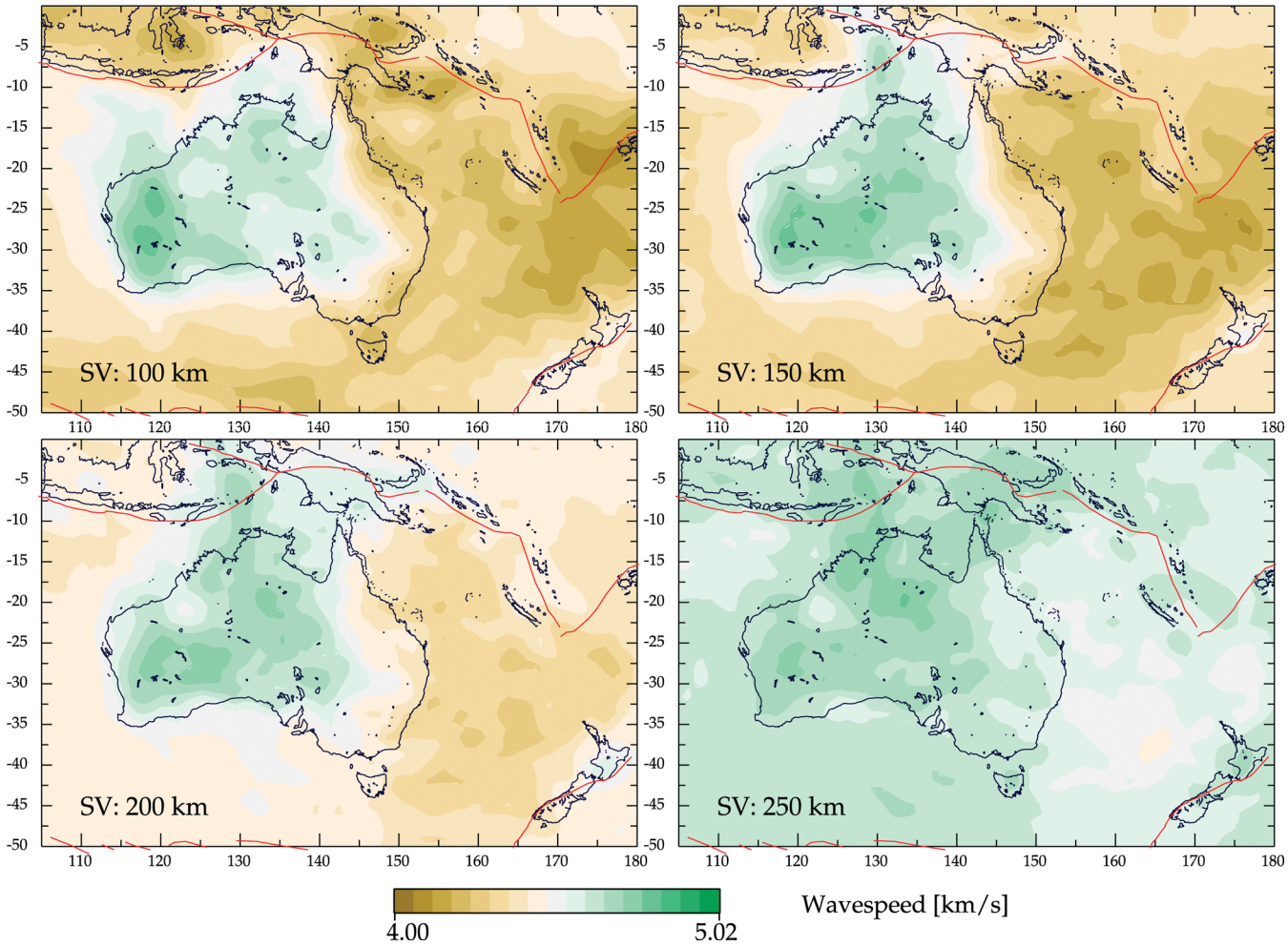

Figure 7. Slices through the AuSREM mantle model for *SV*-wave speed at: 100 km, 150 km, 200 km and 250 km depth.

speed ratio between the models shown in Figs 8 and 7 is rather patchy. In the Appendix we present an alternative construction for an *SH* model utilizing a smooth *SH*/*SV* ratio.

3.2 *P*-wave speed

The main information we have on the *P*-wave speed distribution comes from refracted waves and body wave tomography. The variations in *P*-wave speed in the cratonic lithosphere of Australia are typically between a half and one third of the corresponding *S* variations from the *ak135* model. This provides a useful starting point, but we have been able to incorporate lateral variability in the V_p/V_s ratio to allow for differences between the zones beneath the cratons and the Phanerozoic fold belts. We also have some hints of age dependence between the Archæan and Proterozoic domains.

Building on the results of Kaiho & Kennett (2000), we have represented the variations in the V_p/V_s ratio by scaling the relative deviations $\delta \ln \beta$ in *SV* wave speed from the *ak135* model to produce corresponding *P*-wave speed deviations $\delta \ln \alpha$:

$$\begin{aligned} \delta \ln \alpha &= \delta \ln \beta / [1.875 + (\delta \ln \beta - 0.01) \times 20.0], \quad \delta \ln \beta > 0.01, \\ &= \delta \ln \beta / [1.875 + (\delta \ln \beta - 0.01) \times 2.50], \quad \delta \ln \beta < 0.01. \end{aligned} \tag{3}$$

Then the absolute *P*-wave speed is constructed from

$$\alpha = \alpha_0 (1 + \delta \ln \alpha), \tag{4}$$

where α_0 is the value for the *ak135* model. This simple scheme goes a long way towards capturing the strong effects on *P*-wave speed in areas of reduced *S*-wave speed, and the somewhat muted variations in *P*-wave speed in the higher *S*-wave speed zones.

The resulting *P*-wave speed distribution is shown in Fig. 9 for the same set of depth slices employed for the *SV* and *SH* waves (Figs 7 and 8). At 100 km depth the lowered wave speeds in the Tasman Sea are prominent. The contrast with the continent diminishes with depth.

3.3 Density

We have less direct information on the density in the mantle, apart from the study of Aitken (2010) in which gravity inversion with seismic constraints was used to produce a model of the Moho across Australia. Airy compensation from a depth close to 60 km is largely compatible with the surface gravity results and so we do not need to invoke significant density variations in the upper mantle.

However, if we adopt a simple wave speed–density scaling we will require large densities for the thick cratons, that are incompatible with their buoyant nature in the mantle. Guided by density estimates for different compositions from highly refractory harzburgite to more fertile configurations (S. Klemme, personal communication, 2011), we have constructed an empirical shear wave speed–density relation that compensates for the high cratonic wave speeds in the

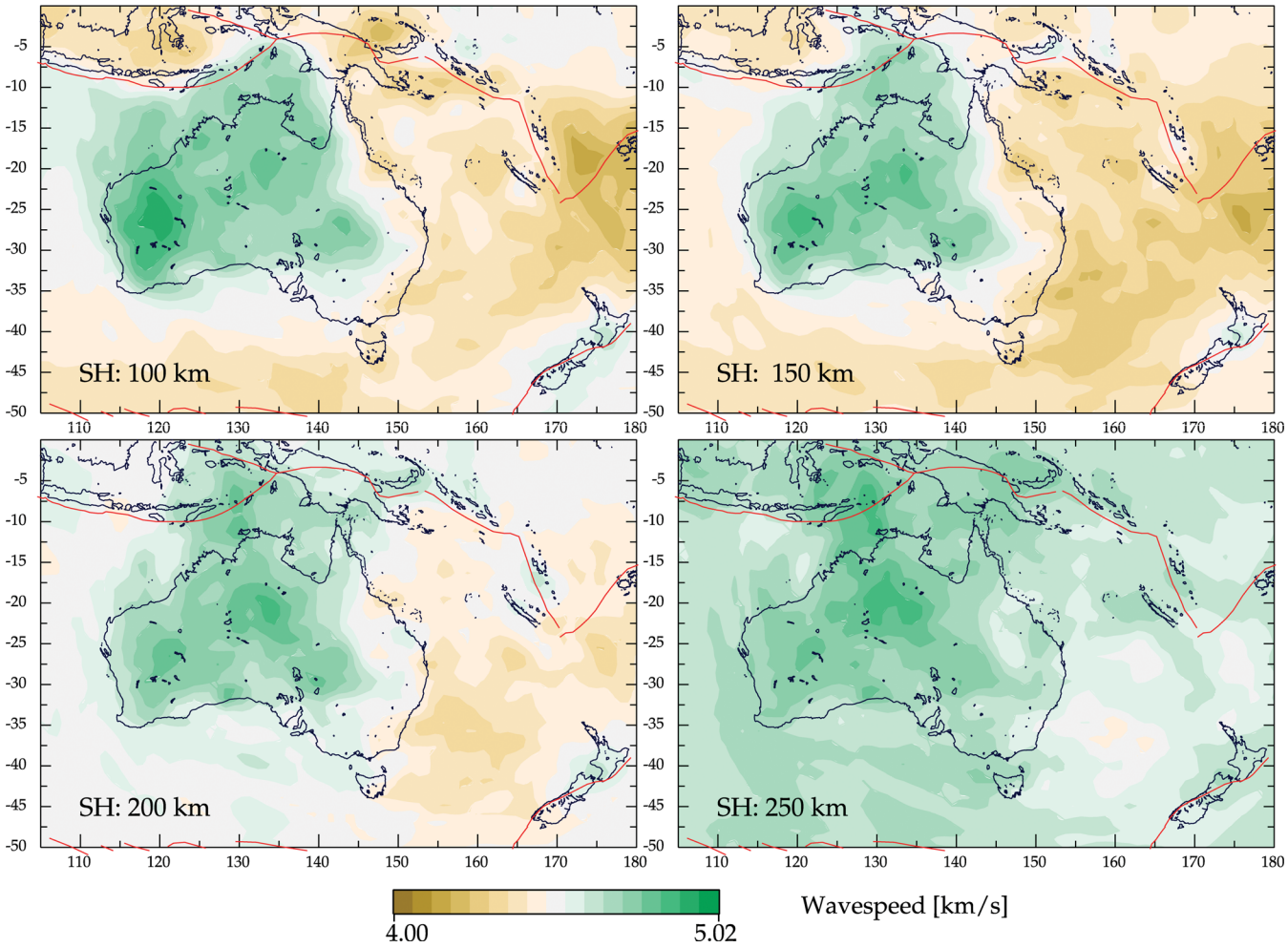

Figure 8. Slices through the AuSREM mantle model for *SH*-wave speed at: 100 km, 150 km, 200 km and 250 km depth.

lithosphere. We set a threshold for the transition to the inclusion of a compositional effect at depth z: $\epsilon = 2.0 + 0.2 \times (z - 50)$ percentage deviation in shear wave speed from the *ak135* model. If the shear wave speed perturbation at a particular depth is less than ϵ per cent, we use a simple scaling of the variation to produce the local density

$$\rho = \rho_0(1 + 0.3 \times \delta \ln \beta), \tag{5}$$

where ρ_0 is taken from *ak135*. For larger perturbations we use a relation with an inverse slope in terms of the absolute *SV* wave speed β,

$$\rho = (13.931 - \beta)/2.7724. \tag{6}$$

Below 180 km we scale back the reduction in density linearly with depth, so that a single representation is applied at 300 km depth.

The two representations link well and we do not see very much of an outline of the fast wave speed zones in the results for density (Fig. 10) except at 200 km where we can readily identify the zone of likely compositional heterogeneity. As can be seen in the plots of the resulting density distribution in Fig. 10, the density contrasts in the mantle are modest and compatible with some degree of thermal input in, for example, the Tasman Sea.

3.4 Transition to the asthenosphere

We can readily recognize the lithosphere beneath the older parts of the continent by fast shear wave speeds (up to 4.7 km s^{-1}), but the transition to the asthenosphere beneath is not generally marked by any sharp transition. Rather there is a gradation from a conductive to a convective regime, most likely linked also to a change in rheology from dislocation to diffusion creep. The presence of the asthenosphere is, however, manifest in enhanced seismic attenuation. The fast lithospheric wave speeds are accompanied by little loss of seismic energy, enabling high-frequency waves for both *P* and *S* to propagate readily from subduction zones into continental Australia (Kennett & Furumura 2008) with extended scattered codas. The high-frequency *S* waves are suddenly lost when the seismic waves penetrate into the asthenosphere, because of its much higher attenuation of shear waves than in the lithosphere (Gudmundsson *et al.* 1994). The effect on *P* waves is significant with a strong change in frequency content, but not as dramatic as for *S*. Kennett & Abdulah (2011) have used the full range of *P*- and *S*-wave arrivals at portable stations across Australia to undertake attenuation tomography that confirms the presence of much stronger attenuation below 210 km depth. Unfortunately we are not able to distinguish between a thin zone of very high attenuation and a broader zone with a less attenuation; so such studies can only provide a broad scale picture of the behaviour.

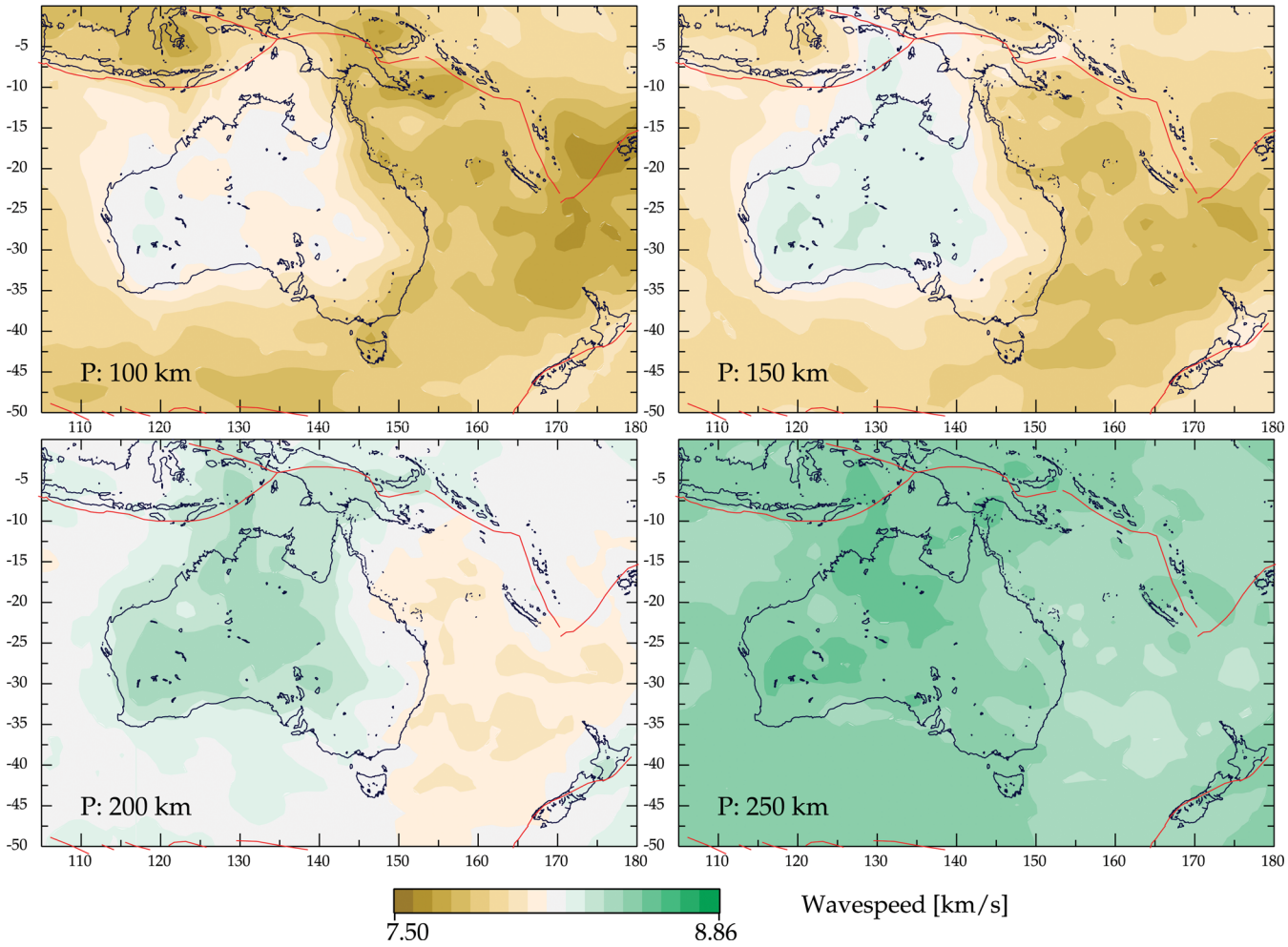

Figure 9. Slices through the AuSREM mantle model for *P*-wave speed at: 100 km, 150 km, 200 km and 250 km depth.

Based on the concept of the transition from a conductive to convective regime we can expect to seek evidence for the transition to the asthenosphere through changes in wave speed gradient. In the absence of a single criterion we have found it effective to use multiple estimators for the location of the base of the lithosphere including the analysis of refracted waves in the mantle, and the wave speeds and gradients deduced from surface wave tomography and body wave tomography. The resulting estimate of the depth to the lithosphere–asthenosphere transition is shown in Fig. 11. The relative variations in the thickness of the lithosphere should be reliable, but the absolute values depend on exactly where the boundary is drawn in a gradational transition. Only in eastern Australia, where the lithosphere is thin, is there *S*-receiver function evidence for a rapid wave speed change (Ford *et al.* 2010). Structure in central Australia is complex, and the gradation of structure with depth is somewhat different than in the rest of the continent (see, e.g. the cross-sections in Fig. 13). It is hard to tell whether, or not, there are localized patches of rather deep penetration of lithospheric material.

The contrast between thick lithosphere in the centre and west and thinner lithosphere in the east is very clear in Fig. 11. The nature of the transition from west to east is consistent with the analysis of Fishwick *et al.* (2008), and it appears that changes in lithosphere thickness can occur over quite narrow zones. Our estimates of the depth to the base of the lithosphere show significant irregularities. This irregular base is likely to impose complex stress patterns in both the lithosphere and asthenosphere associated with the relative motions of the thick continental lithosphere and the freer-flowing asthenosphere. The presence of lithospheric 'steps' will produce complex flows and this has lead Farrington *et al.* (2010) to suggest an edge convection model for the formation of the Newer Volcanic province in Victoria and South Australia that host the most recent eruptions at 4.6 ka. Their concept is that the northward motion of Australia at about 7 cm yr^{-1} gives rise to a trailing flow from the southern edge of the thick cratonic lithosphere that comes to the surface further south creating the volcanic province.

3.5 Attenuation

We have constructed an *S*-wave attenuation model to accompany the wave speed distribution. This Q_β^{-1} model incorporates the very low loss of seismic energy in the cratonic lithosphere (*cf.* Kennett & Furumura 2008), and enhanced asthenospheric loss. We use a single *S*-wave attenuation model. Even though we would expect equivalent polarization anisotropy in attenuation to wave speeds, the differences are rather small (Kennett & Abdulah 2011). The studies of Adbulah (2007) show that the frequency dependence of Q_β^{-1}, at 1 Hz and below, is slight with a frequency exponent less than 0.1, except in the shallow areas of strong attenuation such as the Coral Sea. We have therefore adopted a frequency-independent

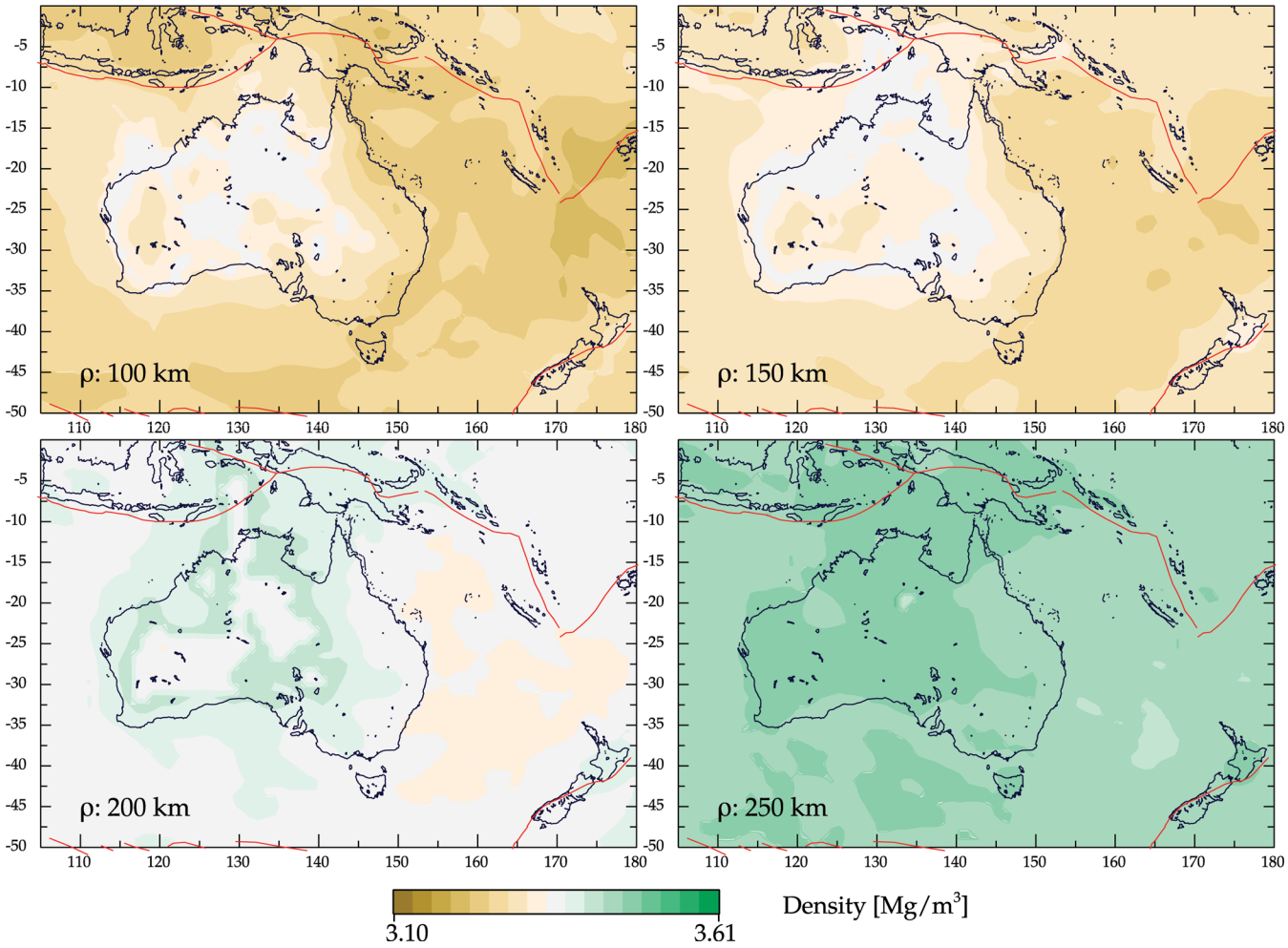

Figure 10. Slices through the AuSREM mantle model for density at: 100 km, 150 km, 200 km and 250 km depth.

attenuation model. *P*-wave attenuation is well represented by a simple scaling $Q_\alpha^{-1} = 0.5 \times Q_\beta^{-1}$.

The attenuation tomography undertaken by Kennett & Abdulah (2011) has highest resolution in the northern part of Australia and towards the Indonesian subduction zone. This model provides important constraints, but the use of stations confined to the continent means that coverage is limited to the east into the Tasman Sea, where surface wave results (Dalton *et al.* 2008) indicate enhanced attenuation ($Q_\beta^{-1} > 0.03$). We have therefore made use of the strong correlation between reduced seismic wave speeds and enhanced attenuation due to the influence of increased temperature or volatiles. The very high *S*-wave speeds found in the cratonic mantle are very hard to explain with temperature alone, and correlate very well with efficient transmission of high-frequency energy from the subduction zones to the north (Kennett & Furumura 2008).

We have therefore made the assumption that a 4 per cent positive perturbation from the *ak135* reference model is associated with $Q_{\beta 0}^{-1} = 0.001$ (i.e. $Q_{\beta 0} = 1000$) within the lithosphere. Down to 200 km depth we then construct the *S*-wave attenuation factor at a horizontal position $\mathbf{x}$ and depth z as

$$Q_\beta^{-1}(\mathbf{x}, z) = Q_{\beta 0}^{-1} \exp\{\zeta[0.04 - \Delta_r\beta(\mathbf{x}, z)]\}, \quad z \le 200 \text{ km}, \qquad (7)$$

where $\Delta_r\beta(\mathbf{x}, z) = [\beta(\mathbf{x}, z) - \beta_0(z)]/\beta_0(z)$ with $\beta_0(z)$ taken from the *ak135* model. Seismic loss then increases rapidly for strong negative $\Delta_r\beta$. The functional relation (7) represents the even faster increase of seismic attenuation than decrease in seismic wave speed as the solidus is approached (Faul & Jackson 2005). The scaling factor ζ has been tuned to match the northern Australian results of Kennett & Abdulah (2011). We have adopted the value $\zeta = 19.0$, which means that seismic attenuation increases 10-fold to $Q_{\beta 0}^{-1} = 0.01$ (i.e. $Q_{\beta 0} = 100$) for a perturbation of -8.12 per cent from *ak135*. In the asthenospheric zone below 200 km, we shift the reference and now require a 10 per cent positive deviation from *ak135* to correspond to $Q_{\beta 0}^{-1} = 0.001$; this corresponds to the change in grain size invoked by Faul & Jackson (2005). The loss factor is then

$$Q_\beta^{-1}(\mathbf{x}, z) = Q_{\beta 0}^{-1} \exp\{\zeta[0.10 - \Delta_r\beta(\mathbf{x}, z)]\}, \quad z > 200 \text{ km}, \qquad (8)$$

with the same scaling factor ζ as before.

This simple empirical scheme reproduces well the attenuation patterns across the Australian continent found by Kennett & Abdulah (2011), yet allows them to be expanded to the full domain of the AuSREM mantle model. In Fig. 12 we show the Q_β^{-1} attenuation distribution derived from the *SV*-wave speed model, for the same set of depth slices as we have used for the other physical parameters.

The strong contrast in seismic attenuation between the cratonic core and the eastern margin of Australia is evident in the 100 km slice. The centres of attenuation on the continent in northern Queensland and Victoria link to recent volcanism. The north Queensland anomaly extends into the Coral Sea, a prominent

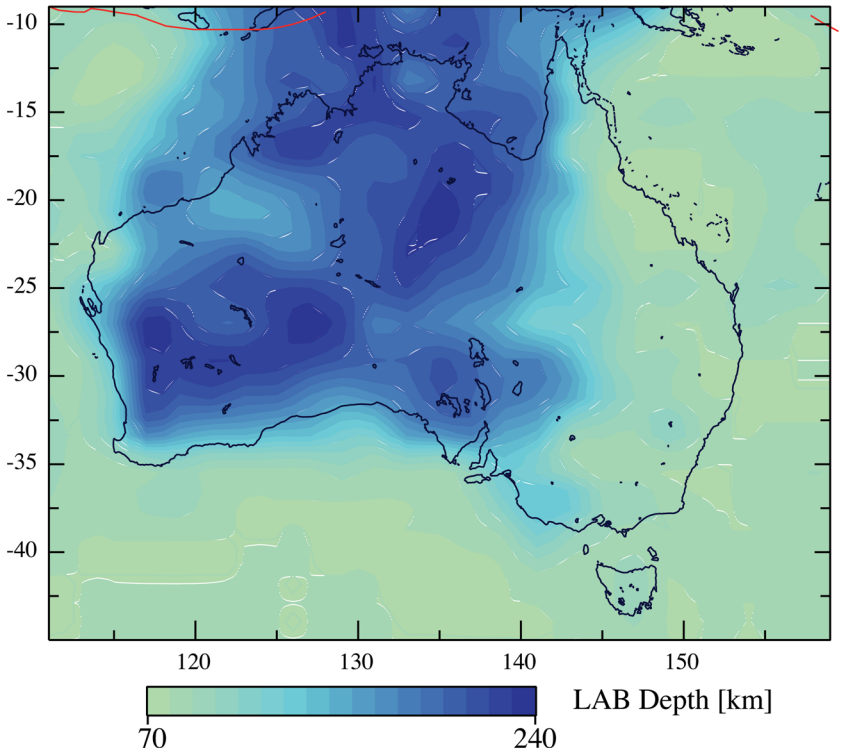

Figure 11. Estimate of the depth to the lithosphere–asthenosphere boundary derived from a combination of different lines of evidence including absolute wave speed and both horizontal and vertical wave speed gradients.

feature in the Kennett & Abdulah (2011) results. There is strong shallow attenuation in the east, notably beneath the Lau Basin, a location of active spreading where $Q_\beta^{-1} > 0.0125$ (i.e. $Q_\beta < 80$) as would be expected in such a hot environment, and in agreement with previous body wave studies (e.g. Flanagan & Wiens 1998; Roth *et al.* 1999). At 150 km depth we see the strong cratonic zone of low loss, bordered to the east by a well-developed higher attenuation corridor and a shallower asthenosphere consistent with early surface wave studies, for example, Goncz & Cleary (1976). At greater depth we see a shift of the whole attenuation distribution to much larger loss of seismic energy, with only a few pockets of lower attenuation associated with cratonic roots (*cf.* Fig. 11).

3.6 External domain

Outside the zone covered by the AuSREM mantle model, we employ the model *S40RTS* of Ritsema *et al.* (2011). Within our model zone the patterns of variation in *S40RTS* are compatible with the larger wavelength features of our model, but the range of wave speeds is somewhat smaller. We have therefore engaged in gentle tapering at the edges of the AuSREM model to ensure a smooth transition into *S40RTS*.

4 DISCUSSION AND CONCLUSIONS

The AuSREM mantle model attempts to provide a representation of the complex pattern of 3-D structure beneath the Australian Plate. The construction of the model has endeavoured to bring in different styles of modelling and inversion, so that the distinctive features of the mantle in the Australian region are adequately captured. For this AuSREM mantle component we use the *SV*-wave speed as the primary control, and have derived the *P*-wave speed, density and shear attenuation from this field. Although we have made a direct construction of an *SH* model, we present an alternative, smoother model derived from the *SV* model in the Appendix.

The most prominent feature of the mantle model is the presence of fast shear wave speeds in the west and centre of Australia compared with the east. This has been a consistent feature as models for the lithospheric mantle under Australia have developed (e.g. Kennett 2003). As can be seen in Figs 3 and 4 this is a a common feature of the three shear wave speed models we have used, and also appears in global models such as *S40RTS* (Ritsema *et al.* 2011) though there the resolution is less.

The effect of increasing temperature is to lower seismic wave speeds. In consequence much of the pattern of wave speeds can be explained by temperature alone, especially where wave speeds are low. Goes *et al.* (2005) attempted to extract temperature from the *SV*-wave speed model of Yoshizawa & Kennett (2004), and were forced to very low temperatures ($<500^\circ$C) in the centre and west, with a very large temperature contrast ($>1000^\circ$C) to the hotter region beneath the Tasman Sea. The exceptionally high wave speeds for *SH* in AuSREM suggest that, as in the study of N. America by Khan *et al.* (2011), compositional heterogeneity is required to achieve the highest shear velocities. This would also be consistent with the very low attenuation observed on paths in cratonic Australia. The lightest tones in the attenuation model in Fig. 12 can thus be expected to outline the area where compositional heterogeneity dominates.

The most common compositional explanation for high seismic velocities is an increase in the Mg#. In central and western Australia this would be quite consistent with the patterns of geochemical variation inferred from inversion of multimode surface wave dispersion for Australia (A. Khan, personal communication). However, it is not clear that a change in Mg# can account for the magnitude of seismic velocity anomaly observed in the reference model. A recent study on the effect of polybaric partial melting indicates maximum

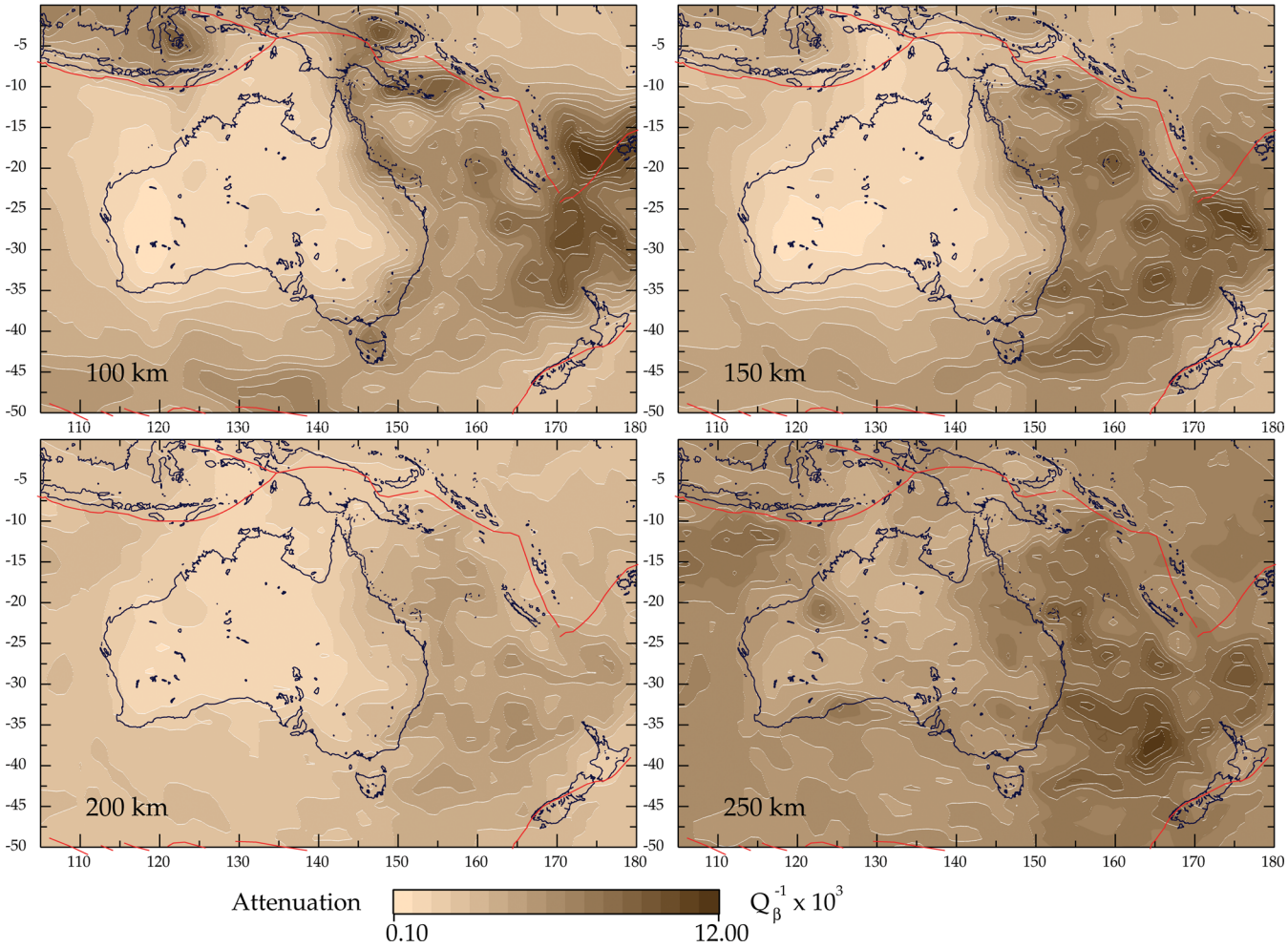

Figure 12. Slices through the AuSREM attenuation model at: 100 km, 150 km, 200 km and 250 km depth.

V_s increases of 1.7 per cent, and only for deep melting paths or high potential temperatures (Afonso & Schutt 2012). These results are in line with previous studies that show the range of velocity variation due to melt depletion to be small, and comparable to the uncertainties in the seismic velocities themselves (e.g. Goes *et al.* 2000). Therefore, while melt depletion is likely to play some role in the high velocities observed beneath much of central and western Australia, further investigation into the maximum amplitude of velocity anomalies is required.

The nature of the mantle model is illustrated in Fig. 13 which shows a group of selected cross-sections through the *SV*-wave speed distribution in both longitude and latitude keyed to a map view at 100 km depth. As in the earlier images we work with absolute velocities, so that there is a natural tendency for the wave speed to increase with depth. Fig. 13 shows very clearly the ambiguities inherent in the choice of a base of the lithosphere. vertical gradients are rather variable, and a criterion that would be very suitable for Western Australia might well be less appropriate for the complex structures in central Australia.

Despite the problems of definition we can recognize a broad pattern in lithospheric thickness that is insensitive to the particular definition employed for the lithosphere–asthenosphere boundary (*cf.* Fig. 11). The cratonic region in the centre and west of Australia is underlain by a thick mantle lithosphere extending to over 200 km depth with fast wave speeds (especially for shear waves). Beneath the Tasman Fold Belt in the east, a region of younger Phanerozoic upper crust, the lithosphere is generally thinner (less than 140 km) and the asthenosphere has a pronounced low-velocity zone for shear waves with high attenuation of shear wave energy.

The centre of Australia has relatively low wave speeds at 75 km (Figs 13 and 14), but there are strong gradients with depth and by 125 km a broad zone of fast wave speeds is established across the centre and west of Australia that persists to more than 200 km depth (Figs 5, 11 and 13). Lower seismic wave speeds are also seen in the Canning Basin area to some depth. These are the two regions that have seen the most recent deformation. Elsewhere, the ancient continental core of Australia in the centre and west of the continent is marked by relatively high seismic wave speeds throughout the lithosphere (Fig. 14).

In contrast in the Tasman Fold belt to the east, the seismic wave speeds in the mantle are somewhat lower and the lithosphere is relatively thin, with estimates around 80 km. The Tasman Sea region displays quite low shear wave speeds (down to 4.2 km s^{-1}), probably as a result of residual heat left from failed rifting around 80 Ma (Fig. 13). Fishwick *et al.* (2008) have presented evidence for the progressive eastward thinning of the lithosphere across Australia, which occurs as a series of discrete steps with quite sharp transitions. This result poses interesting questions as to how such lithospheric steps can be maintained over extended periods of geological time.

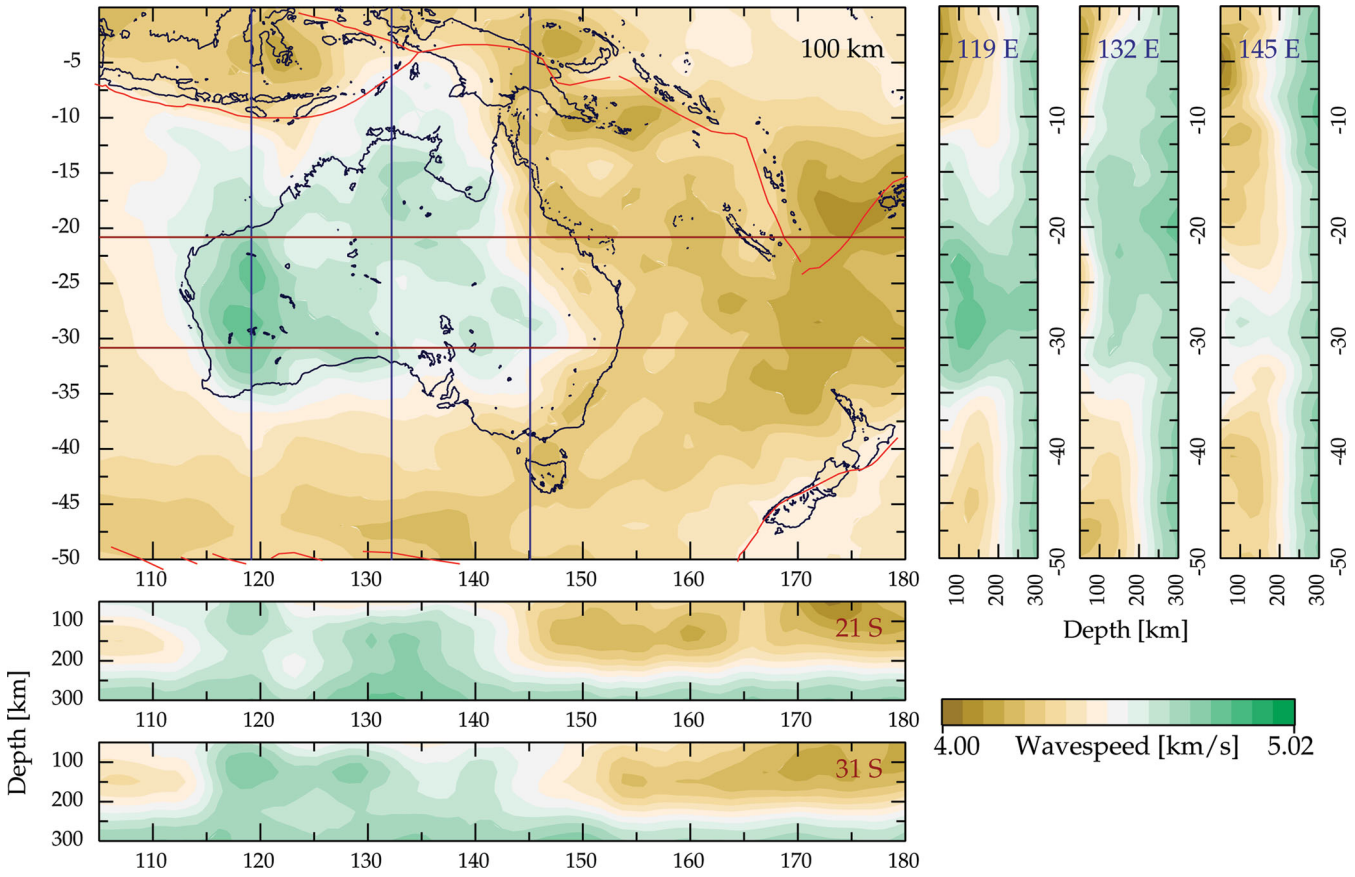

Figure 13. Cross-sections through the *SV*-wave speed component of the AuSREM mantle model along the lines indicated on the key map showing the a map view at 100 km depth. Sections are shown at 21°S, 31°S and at 119°E, 132°E, 145°E. Note, as in the depth slices, the colours represent absolute wave speed so that an increase with depth is to be expected.

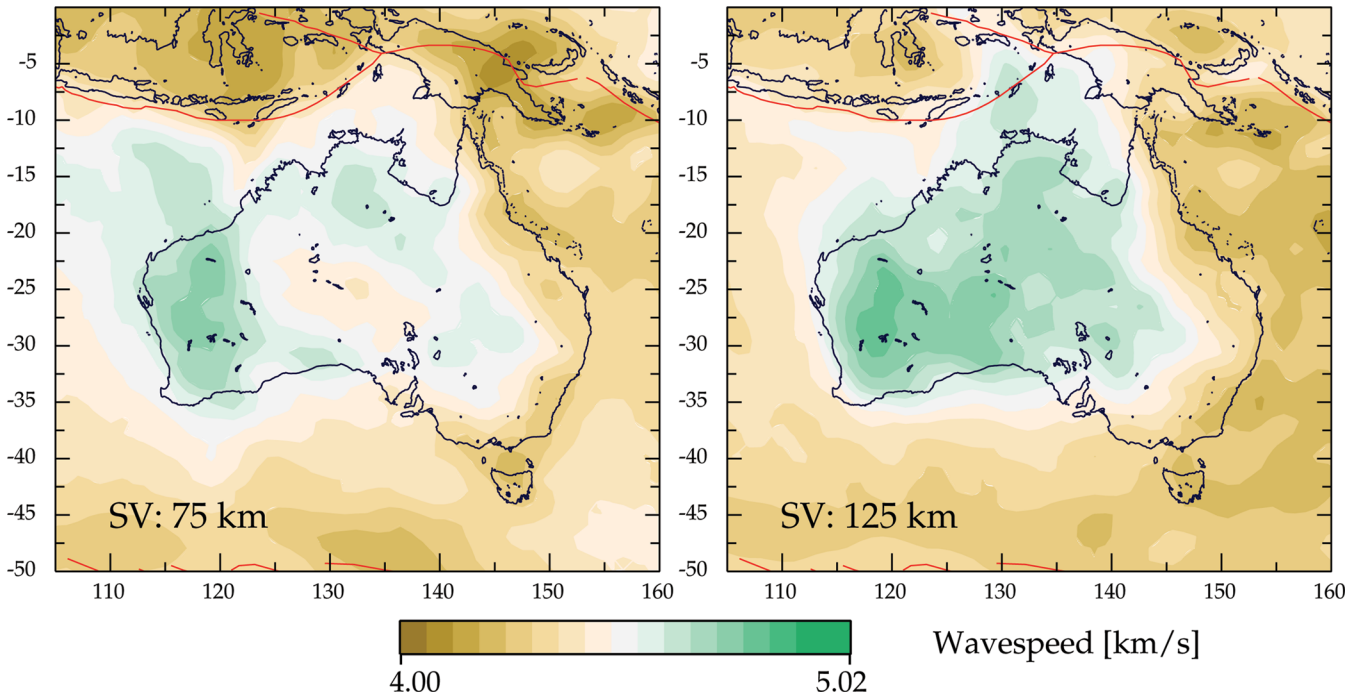

Figure 14. Comparison of *SV*-wave speed at 75 km and 125 km depth.

The complete AuSREM model with both crustal and mantle provides a representation of 3-D structure beneath Australia and its environs at a common 0.5° sampling that can be used for many purposes. Both the crustal and mantle components should be useful in gravity modelling and in studies of dynamic topography. The crustal component provides corrections for future mantle studies for both surface wave tomography and delay time tomography on a finer scale. Tools are under active development for location of earthquakes in the full 3-D model, and for earthquake source characterization.

5 THE AuSREM MODEL

The AuSREM model is presented in full at the website http://rses.anu.edu.au/seismology/AuSREM from which the model can be downloaded in a number of formats, and where it is also possible to generate maps and depth profiles.

ACKNOWLEDGMENTS

The AuSREM project has been jointly supported by AuScope and the Research School of Earth Sciences, Australian National University. Funding support for the passive seismic work in Australia has been provided from the Australian National University, from Discovery Projects funded by the Australian Research Council, from the Predictive Mineral Discovery Cooperative Research Centre, and the AuScope infrastructure initiative. Prof S. Klemme is thanked for discussions on mantle density.

REFERENCES

Abdulah, A., 2007. Seismic body wave attenuation tomography beneath the Australasian region, *PhD thesis,* Australian National University.

Afonso, J.C. & Schutt, D.L., 2012. The effects of polybaric partial melting on density and seismic velocities of mantle restites, *Lithos,* **134–135,** 289–303.

Aitken, A.R.A., 2010. Moho Geometry Gravity Inversion Experiment (MoGGIE): a refined model of the Australian Moho, and its tectonic and isostatic implications, *Earth planet. Sci. Lett.,* **297,** 71–83.

Cara, M. & Lévêque, J., 1987. Waveform inversion using secondary observables, *Geophys. Res. Lett.,* **14,** 1046–1049.

Dalton, C.A., Ekström, G. & Dziewoński, A.M., 2008. The global attenuation structure of the upper mantle, *J. geophys. Res.,* **113**(B09303), doi:10.10292007JB005429.

Debayle, E. & Kennett, B.L.N., 2003. Surface wave studies of the Australian region, in *The Evolution and Dynamics of the Australian Plate,* pp. 25–40, eds Müller, D. & Hillis, R., Geological Society of Australia Special Publication 22 and Geological Society of America Special Paper 372, Sydney.

Debayle, E., Kennett, B.L.N. & Priestley, K., 2005. Global azimuthal seismic anisotropy and the unique plate-motion deformation of Australia, *Nature,* **433,** 509–512.

Direen, N.G. & Crawford, A J., 2003. The Tasman Line: where is it, what is it, and is it Australia's Rodinian breakup boundary?, *Austral. J. Earth Sci.,* **50,** 491–502.

Farrington, R., Stegman, D., Moresi, L.N., Sandiford, M. & May, D., 2010. Interactions of 3D mantle flow and continental lithosphere near passive margins, *Tectonophysics,* **483,** 20–28.

Faul, U. & Jackson, I., 2005. The seismological signature of temperature and grain size variations in the upper mantle, *Earth planet. Sci. Lett.,* **234,** 119–234.

Fichtner, A. & Igel, H., 2008. Efficient numerical surface wave propagation through the optimization of discrete crustal models: a technique based on non-linear dispersion curve matching (DCM), *Geophys. J. Int.,* **173,** 519–533.

Fichtner, A., Kennett, B.L.N., Igel, H. & Bunge, H.-P., 2009. Full seismic waveform tomography for upper-mantle structure in the Australasian region using adjoint methods, *Geophys. J. Int.,* **179,** 1703–1725.

Fichtner, A., Kennett, B.L.N., Igel, H. & Bunge, H.-P., 2010. Full seismic waveform tomography for radially anisotropic structure: new insights into the past and present states of the Australasian upper mantle, *Earth planet. Sci. Lett.,* **290,** 270–280.

Fichtner, A., Fishwick, S., Yoshizawa, K. & Kennett, B.L.N., 2012. Optimal spherical spline filters for the analysis and comparison of regional-scale tomographic models, *Phys. Earth planet. Inter.,* **190,** 44–50.

Fishwick, S. & Rawlinson, N., 2012. 3-D structure of the Australian lithosphere from evolving seismic datasets, *Aust. J. Earth Sci.,* **59,** 809–826.

Fishwick, S., Kennett, B.L.N. & Reading, A.M., 2005. Contrasts in lithospheric structure within the Australian Craton, *Earth planet. Sci. Lett.,* **231,** 163–176.

Fishwick, S., Heintz, M., Kennett, B.L.N., Reading, A.M. & Yoshizawa, K., 2008. Steps in lithospheric thickness within eastern Australia, evidence from surface wave tomography, *Tectonics,* **27**(TC0049), doi:10.129/2007TC002116.

Flanagan, M.P. & Wiens, D.A., 1998. Attenuation of broadband *P* and *S* waves in Tongas: observations of frequency dependent Q, *Pure appl. Geophys.,* **153,** 345–375.

Ford, H.A., Fischer, K.M., Abt, D.L., Rychert, C.A. & Elkins-Tanton, L.T., 2010. The lithosphere-asthenosphere boundary and cratonic lithospheric layering beneath Australia from *Sp* wave imaging, *Earth planet. Sci. Lett.,* **300,** 299–310.

Goes, S., Govers, R. & Vacher, P., 2000. Shallow mantle temperatures under Europe from *P* and *S* wave tomography, *J. geophys. Res.,* **105,** 11 153–11 169.

Goes, S., Simons, F.J. & Yoshizawa, K., 2005. Seismic constraints on temperature of the Australian uppermost mantle, *Earth planet. Sci. Lett.,* **236,** 227–237.

Goncz, J.H. & Cleary, J.R., 1976. Variations in the structure of the upper mantle beneath Australia, from Rayleigh wave observations, *Geophys. J. R. astr. Soc.,* **44,** 507–516.

Gorbatov, A. & Kennett, B.L.N., 2003. Joint bulk-sound and shear tomography for Western Pacific subduction zones, *Earth planet. Sci. Lett.,* **210,** 527–543.

Gudmundsson, O., Kennett, B.L.N. & Goody, A., 1994. Broadband observations of upper mantle seismic phases in northern Australia and the attenuation structure in the upper mantle, *Phys. Earth planet. Inter.,* **84,** 207–236.

van der Hilst, R., Kennett, B.L.N., Christie, D. & Grant, J., 1994. Project SKIPPY explores the lithosphere and mantle beneath Australia, *EOS, Trans. Am. geophys.Un.,* **75,** 177.

Kaiho, Y. & Kennett, B.L.N., 2000. Three-dimensional seismic structure beneath the Australasian region from refracted wave observations, *Geophys. J. Int.,* **142,** 651–668.

Kennett, B.L.N., Engdahl, E.R. & Buland, R., 1995. Constraints on seismic velocities in the Earth from travel times, *Geophys. J. Int.,* **122,** 108–124.

Kennett, B.L.N., 2003. Seismic structure in the mantle beneath Australia, in *The Evolution and Dynamics of the Australian Plate,* pp. 7–23, eds Müller, D. & Hillis, R., Geological Society of Australia Special Publication 22 and Geological Society of America Special Paper 372, Sydney.

Kennett, B.L.N. & Abdulah, A., 2011. Seismic wave attenuation beneath the Australasian region, *Aust. J. Earth. Sci.,* **58,** 285–295.

Kennett, B.L.N. & Furumura, T., 2008. Stochastic waveguide in the lithosphere: Indonesian subduction zone to Australian Craton, *Geophys. J. Int.,* **172,** 363–382.

Kennett, B.L.N. & Salmon, M., 2012. AuSREM: The Australian Seismological Reference Model, *Aust. J. Earth. Sci.,* doi:10.1080/08120099.2012.736406.

Kennett, B.L.N., Salmon, M., Saygin, E. & AusMoho Working Group, 2011. AusMoho: the variation of Moho depth in Australia, *Geophys. J. Int.,* **187,** 946–958.

Khan, A., Zunino, A. & Deschamps, F., 2011. The thermo-chemical and physical structure beneath the North American continent from Bayesian

inversion of surface-wave phase velocities, *J. geophys. Res.,* **116**(B09304), doi:10.1029/2011JB008380.
Molinari, I. & Morelli, A., 2011. EPcrust: a reference crustal model for the European plate, *Geophys. J. Int.,* **185,** 352–364.
Rawlinson, N., Kennett, B.L.N., Vanacore, E., Glen, R.A. & Fishwick, S., 2011. The structure of the upper mantle beneath the Delamerian and Lachlan orogens from simultaneous inversion of multiple teleseismic datasets, *Gondwana Res.,* **20,** doi:10.1016/j.gr.2010.11.001.
Ritsema, J., Deuss, A., van Heijst, H.J. & Woodhouse, J.H., 2011. S40RTS: a degree-40 shear-velocity model for the mantle from new Rayleigh wave dispersion, teleseismic traveltime and normal-mode splitting function measurements, *Geophys. J. Int.,* **184,** 1223–1236.
Roth, E.G., Wiens, D.A., Dorman, L.M., Hildebrand, J. & Webb, S.C., 1999. Seismic attenuation tomography of the Tonga-Fiji region using phase pair methods, *J. geophys. Res.,* **104,** 4795–4809.
Salmon, M., Kennett, B.L.N. & Saygin, E., 2012. Australian Seismological Reference Model (AuSREM): crustal component, *Geophys. J. Int.,* doi:10.1093/gji/ggs004.
Sambridge, M.S., 1999. Geophysical inversion with a neighbourhood algorithm: I. Searching a parameter space, *Geophys. J. Int.,* **138,** 479–494.
Schivardi, R. & Morelli, A., 2011. EP mantle: a three-dimensional transversely isotropic model of the upper mantle under the European Plate, *Geophys. J. Int.,* **185,** 469–484.
Simons, F.J., Van Der Hilst, R.D., Montagner, J.-P. & Zielhuis, A., 2012. Multimode Rayleigh wave inversion for heterogeneity and azimuthal anisotropy of the Australian upper mantle., *Geophys. J. Int.,* **151,** 738–754.
Yoshizawa, K. & Ekström, G., 2010. Automated multimode phase speed measurements for high-resolution regional-scale tomography: application to North America, *Geophys. J. Int.,* **183,** 1538–1558.
Yoshizawa, K. & Kennett, B.L.N., 2002. Non-linear waveform inversion for surface waves with a neighbourhood algorithm: application to multimode dispersion measurements, *Geophys. J. Int.,* **149,** 118–133.
Yoshizawa, K. & Kennett, B.L.N., 2004. Multi-mode surface wave tomography for the Australian region using a 3-stage approach incorporating finite frequency effects, *J. geophys. Res.,* **109**(B02310), doi: 10.129/2002JB002254.

APPENDIX: ALTERNATIVE CONSTRUCTION OF *SH* MODEL

For the *SH*-wave speed model shown in Fig. 8 we employed information from the two recent *SH* models. As noted, this lead to a rather patchy distribution of the *SH*/*SV* wave speed ratio. For a representative model we would prefer that all components of the model are at a comparable level of smoothness, which is why we have used the *SV* model in the construction of the *P*-wave speed, density and Q^{-1} models.

We can take a comparable approach for *SH* by utilizing a smooth *SH*/*SV* wave speed distribution taken from the study with the broader geographic path coverage (Yoshizawa, personal communication, 2012). The pattern of the wave speed ratio is illustrated in Fig. A1, and the *SH*-wave speed model constructed using this ratio applied to the AuSREM *SV* model is shown in Fig. A2. Comparison of Figs 8

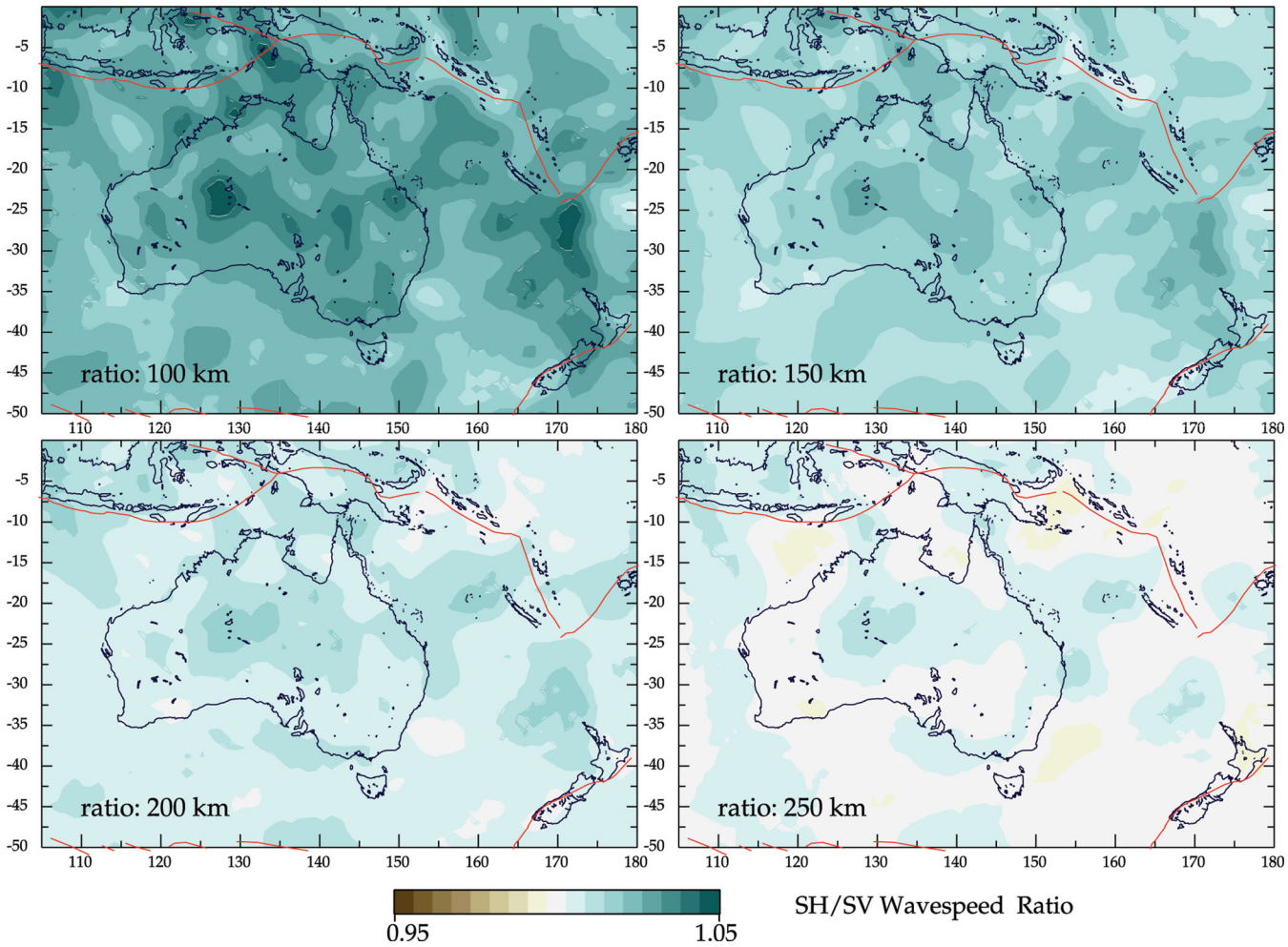

Figure A1. Slices through the smoothed *SH*/*SV* wave speed ratio in the mantle at: 100 km, 150 km, 200 km and 250 km depth.

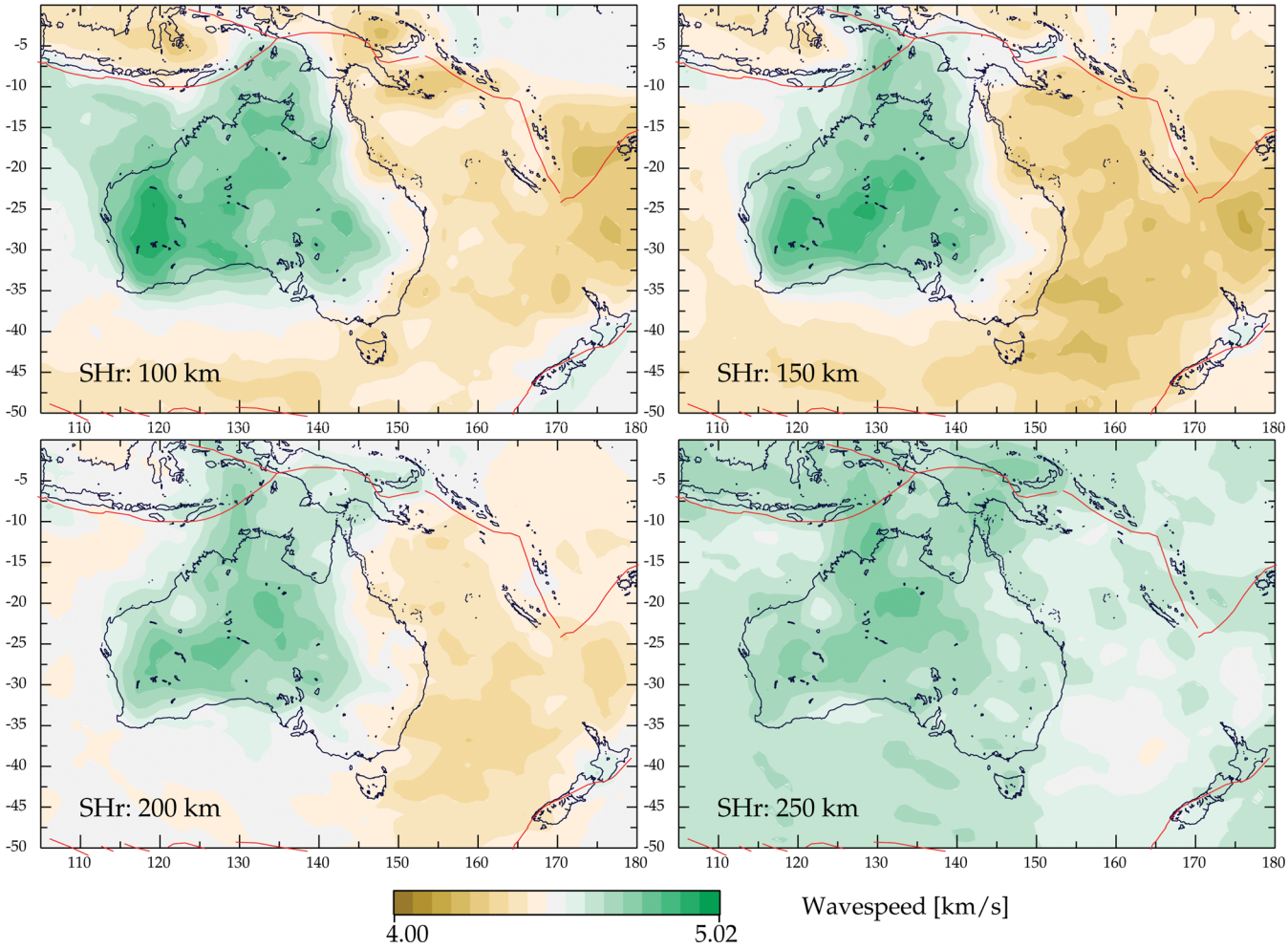

Figure A2. Slices through the alternative AuSREM mantle model for *SH* wave speed, constructed from the *SV* model (Fig. 7) with the application of the *SH*/*SV* ratio from Fig. A1, at: 100 km, 150 km, 200 km and 250 km depth.

and A2 indicates that we have captured much of the character of the original *SH* model, but with slightly less heterogeneity at depth.

SUPPORTING INFORMATION

Additional Supporting Information may be found in the online version of this article.

(http://gji.oxfordjournals.org/lookup/supp1/doi:10.1093/gji/ggs065/-/DC1)

Please note: Oxford University Press is not responsible for the content or functionality of any supporting materials supplied by the authors. Any queries (other than missing material) should be directed to the corresponding author for the article.